Numerical analysis of the Hydrodynamic Ram phenomenon in aircraft fuel tanks

D. Varas[1] and J. López-Puente[2] and R. Zaera[3]
University Carlos III of Madrid. Avda. de la Universidad, 30. 28911 Leganés, Madrid, Spain

Hydrodynamic Ram (HRAM) is a phenomenon that occurs when a high-energetic object penetrates a fluid-filled container. The projectile transfers its momentum and kinetic energy through the fluid to the surrounding structure increasing the risk of catastrophic failure and an excessive structural damage on adjacent components. It is of particular concern in the design of wing fuel tanks for aircraft because it has been identified as one of the important factors in aircraft vulnerability. In order to study the aforementioned phenomenon, water filled aluminium tubes (to different volume percentages) were subjected to impact of spherical projectiles. This work is focused on the analysis of energies, momenta and pressure contours obtained by means of a previously developed and validated numerical model in order to achieve a better understanding of the fluid/structure interaction problem that takes place during the HRAM phenomenon.

I. Introduction

The process by which a high-speed projectile penetrates a fluid-filled tank and transfers kinetic energy to the surrounding walls is known as Hydrodynamic Ram (HRAM). The HRAM effect in fuel tanks is identified as one of the important factors in aircraft vulnerability because the fuel tanks represent the largest exposed area of all the vulnerable components. HRAM is particularly

---

[1] Associate Professor, Department of Continuum Mechanics and Structural Analysis.
[2] Associate Professor, Department of Continuum Mechanics and Structural Analysis.
[3] Professor, Department of Continuum Mechanics and Structural Analysis.

dangerous for aircrafts with lightweight designs, because the structural resistance of their integral fuel tanks cannot be improved by strengthening the airframe. Strengthening the frame would counteract the requirements of a lightweight design. Studies by government agencies and aircraft manufacturers show that the cost of installing countermeasures or strengthtening the aircraft to defend against these threats is inapplicable for cost reasons. Therefore, it becomes necessary to determine the damage caused by these projectiles, to enable the development of techniques to safely land the damaged aircraft using the remaining systems [1].

Vulnerability to HRAM is usually, but not exclusively, related to military aircraft. In 1990 the Federal Aviation Administration (FAA) established the Aircraft Catastrophic Failure Prevention Research Program. The program considered that commercial aircrafts are at risk due to high velocity impacts, so the analysis of the effects of an uncontained turbine engine fragment penetrating aircraft fuel tanks was carried on [2]. Another example of the effect of an impact in a fuel tank of a commercial aircraft happened in the year 2000, when a Concorde crashed after takeoff from Charles de Gaulle airport (France). The final investigation report revealed that the HRAM had played a significant role in the aircraft failure.

Hydrodynamic Ram consists of four principal stages: shock, drag, cavitation and exit. Each stage contributes to structural damage through a different mechanism and to a different extent. When the projectile penetrates the wall of the fluid filled structure, the impact energy is transferred to the fluid and generates a high-pressure hemispherical shock wave. This leads to damage primarily in the vicinity of the impact position. During the drag phase, the projectile travels through the fluid, and its kinetic energy is partially transformed into fluid motion as the projectile is slowed by viscous drag. The displacement of the fluid from the projectile path generates a radial pressure field. In contrast to the pressure field developed during the shock phase, the fluid is accelerated gradually rather than impulsively. This causes less intense peak pressures, but they are of greater temporal extent. The displacement of fluid during the drag stage forms a cavity behind the projectile. The subsequent expansion and collapse (oscillations) of the cavity is known as the cavitation stage. The oscillations of the cavity can cause significant pressure pulses. The final stage of Hydrodynamic Ram occurs when the projectile exits the container. In contrast to the perforation of the front wall,

the exit of the projectile occurs through a pre-stressed wall. The pre-stress is caused by the initial shock stage and the subsequent loading by the fluid.

The military industry has always been interested in the protection of the fuel tanks. In the 1970s, various groups within the US Defense Department expended a considerable research effort to achieve a better understanding of the HRAM phenomenon and the associated fluid-structure interaction problem. The Naval Weapons Center (NWC, China Lake, California), conducted an interesting HRAM project in which a series of ballistic tests were performed to obtain fluid pressure measurements at several locations for a variety of projectiles [3]. A digital computer code for predicting the drag phase fluid pressure in a rectangular tank due to ballistic penetrators, based upon the theory and the empirical data of Lundstrom et al. [3, 4], was subsequently developed by Lundstrom and Fung [5]. The second phase of the same project involved the characterization of the fluid-structure interaction during the loading of the fuel tank walls by the HRAM pressure [6]. Description of the tests and their results are reported in refs. [7–17]. The University of Dayton Research Institute also performed several impact experiments on fuel tanks during the 1970s. S.J. Bless et al. [18] carried out experiments using spherical projectiles of 11.1 and 14.3 mm diameter with a velocity range of 1.5 to 2.4 km/s and obtained data for the entrance and side panel displacement, fluid pressure and the projectile trajectory. In all the mentioned works, the fluid-filled container consisted of a structure on which different panels could be placed and the top of the tank was always open. The aforementioned works are probably some of the first studies of HRAM, but some others can be found [19–24]. Recently, some authors analysed the HRAM phenomenon through the results of intrumented experimental tests. Lecysyn et al. [25–27] studied the drag and cavitation phases of the hydraulic ram, reporting measurements of the movement and deceleration of a projectile after it impacts a fluid-filled vessel results. Disimile et al. [28–30] applied a large-scale shadowgraph technique to a fuel tank simulator in order to visualize the pressure waves generated by hydrodynamic ram, and the results were compared to pressure transducer signals; special attention was given to the effect of the succesive cavity implosions. The same authors installed different geometries of triangular bars to provide shock wave mitigation of the internal pressures.

In addition to the experimental programs, simulation of HRAM events was accomplished. The

first methods were based on the use of the *Piston Theory* [31, 32] and the *Variable Image Method* [33] for the fluid-structure interaction. In general, none of these methodologies provided a realistic coupling between the fluid and the structure. Other codes such as HRSR (Hydraulic Ram Structural Response) [34], ERAM or EHRSR were developed [35], but all of them shown their limitations on simulating an HRAM event. The complicated physics and mechanics of HRAM phenomena were not satisfactory solved until higher-order numerical algorithms were incorporated into the codes in the late 1980s. The Coupled Euler-Lagrange methods have been under development since the early-to-mid 1990s, combining the desirable characteristics of Lagrangian and Eulerian formulations. These methods are used in multiple industries for a wide variety of analysis in which fluids interact with structures or when high distortions may appear [2, 22, 36–42], including airbag and tire-water dynamics in the automobile field [43, 44], the impact of bird strikes on aircraft [45, 46], and the effects of sloshing on ships [47]. The Arbitrary Lagrangian Eulerian (ALE) technique is widely used in those kind of problems. Recently, Sauer [48] presented a numerical study on the simulation of impacts of projectiles on fluid-filled containers. Two different numerical approaches are compared which are both implemented in a research hydrocode: a pure Lagrangian discretization with Finite Elements (FE) and element erosion, and a coupled adaptive FE/SPH discretization. The results showed a better agreement with experimental results by using the adaptive SPH approach. However, the price that currently has to be paid are higher calculation times. In the last years, there have been new advances in development and use of computational methods for fluid-structure interactions due to the interest of reaching more effective computational techniques [49–54] and solving more difficult problems motivated by different industries, such as aeronautics, naval or more recently biomedical sciences. The HRAM phenomenon has also been investigated on composite structures [55].

In a previous work of the authors [56] experimental results were performed to obtain detailed information on the projectile deceleration, cavity evolution, pressure within the fluid and deformation of the tank walls. Later on [57, 58] fully coupled numerical models were developed to simulate the problem; these models were validated with experimental results, faithfully reproducing them, and the most appropriate techniques to simulate the HRAM phenomenon were pointed out. In the present work the simulation methodology, previously developed and validated, is used to analyze

the fluid/structure interaction phenomenon that takes place during HRAM, taking advantage of the broad range of quantitative results that the numerical code can provide. The impact of steel spherical projectiles on aluminium square tubes filled to different volume percentages is simulated. The link between projectile advance and deformation of the tank is established by means of a study of the interactions between these two solids and the fluid. A detailed analysis of the transfer of energy and momentum between projectile, fluid and recipient allowed to identify the beginning and the end of each stage of the HRAM, and their influence in the permanent displacement of the structure.

II. Problem description and Finite element model

In order to analyze the HRAM effects and the associated fluid-structure interaction problem in a structural element representative of a wing fuel cell, aluminium tubes filled with water were impacted by a steel sphere with a diameter of 12.5 mm and a mass of 8 g. The tubes, filled with water to different volume fractions 60, 75 and 100%, were impacted at different velocities: 600 and 900 m/s.

The tanks consisted of 6063-T5 square section aluminium tubes with the following dimensions: 750 mm long, 150 mm wide and 2.5 mm thick. The specimens were closed with two PMMA windows 30 mm thick, fixed to the specimen with four steel bars (Fig. 1); these transparent panels allowed for the video recording of the impact process. Further details about experiments, both set-up and results can be found in [56].

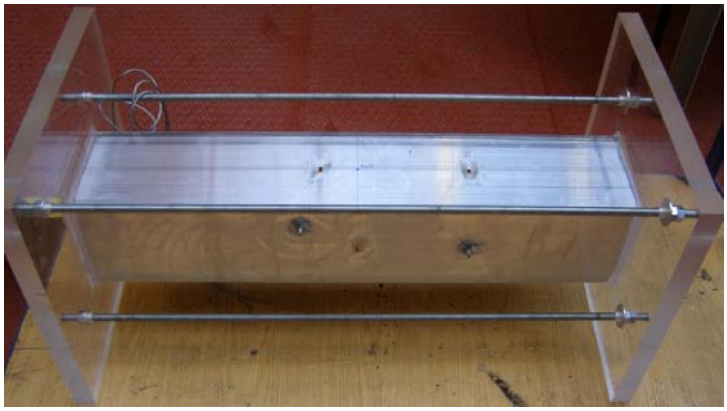

Fig. 1 Aluminium tank.

The numerical model was developed on the commercial finite element code LS-DYNA v.971.

This software is particularly suitable for nonlinear dynamic problems, such as impacts or explosions. It also allows the employment of different techniques such as ALE or SPH to solve fluid and fluid-structure problems. On this paper, the ALE technique was adopted to obtain the results that will be analyzed later.

A. Tank and projectile FE model.

The problem that is going to be modeled can be simplified attending the symmetries. When the tubes are partially filled, only half of the whole geometry needs to be taken into account (Fig. 2, Left). The cases in which the tubes are completely filled, the model can be reduced to a quarter of the whole geometry (Fig. 2, Right). Since the nature of this simulation demands a very high mesh density, such a reduction in the model size is very desirable. The tank has been divided in three parts, the walls impacted by the projectile (entry and exit walls), the lateral walls and the PMMA window.

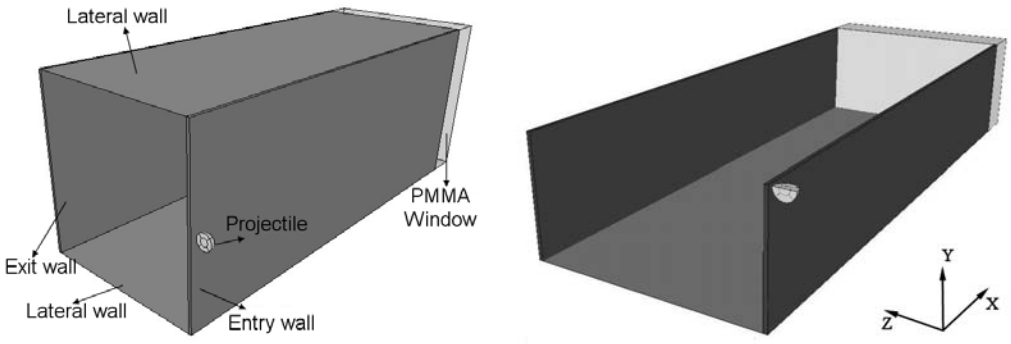

Fig. 2 Box model geometry used. Left: partially filled tube case. Right: completely filled tube case.

The impacted walls and the PMMA window were discretized by means of eight-node solid hexahedron Lagrangian elements with reduced integration. The impacted walls present 5 elements through the thickness and elements of 1 mm in size in the other two directions near the impacted zone. Based on previous simulations, the mesh size was considered appropriate to reproduce the behavior of the solids in the impacted zone. Four-node Belytschko-Tsay shell elements were used to discretize the lateral walls in order to reduce the number of elements. Finally, the mesh of the box consisted of 31804 elements.

The aluminium tubes were modeled by means of the Johnson-Cook thermoviscoplastic hardening relation [59]. The required parameters for the Aluminium 6063-T5 were obtained from Yang [61] and Karagiozova and Jones [60, 61]. In order to describe the material failure in the zone around the impact point, an erosion criterion based on a critical value of the equivalent plastic strain $\varepsilon_f = 0.2$ was adopted.

An elastic material model was used for the PMMA window and the steel projectile since none of them suffered plastic deformations nor damage. The PMMA properties were obtained from Vesenjak et al. [62]. The projectile was discretized by means of eight-nodes solid hexaedron Lagrangian elements with reduced integration. The elements size of the projectile, although relatively bigger than that of the wall elements in the impact area, allows to solve in a properly way the contacts with the tank walls. The material parameters used are detailed in Varas et al. [57].

B. Model for the Fluid

As a result of the HRAM phenomenon, the fluid inside the tank undergoes too large deformations to consider a pure Lagrangian description as an appropriate option. For this reason, a multi-material ALE formulation with a second order accurate advection method has been chosen for the treatment of the fluid. The ALE formulation allows the motion of the mesh independently of the material flow without distortion problems.

Fluids inside and outside the tank (water and air) are discretized by means of eight-node solid hexahedron elements with an ALE formulation. It is necessary to model the air surrounding the tube in order to allow the water to flow into it, and so deforming the walls of the structure. To achieve that, water and air meshes have to share the same nodes at their interfaces. Four discretization densities were analyzed in order to achieve an optimal fluid mesh density. It was found that the finer meshes presented instability and leakage problems at the fluid/solid interfaces. To avoid these problems, numerous iterations modifying some of the coupling parameters were made, and finally it was decided to modify the mesh size in order to match the Lagrangian one at the interfaces. This change in the mesh helped to control the leakage problems. Finally, the fluid mesh has 123038 elements in the partially filled tube cases and 61519 in the completely filled ones (Fig. 3).

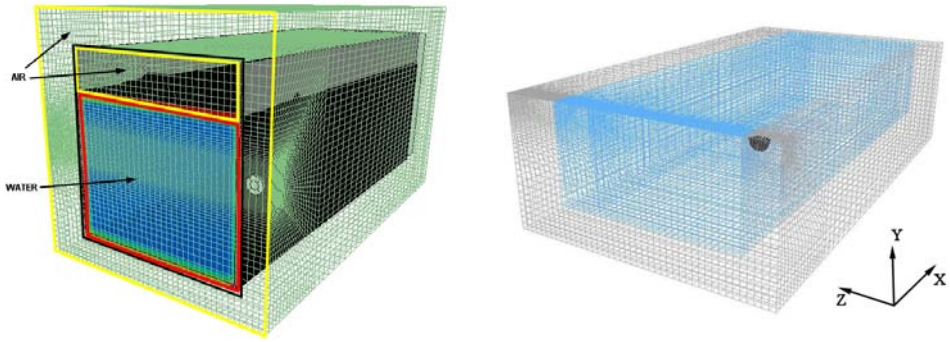

Fig. 3 Mesh of the fluids. Left: partially filled tube. Right: completely filled tube.

The water was modeled using a viscous constitutive equation in which the stress tensor is a function of the dynamic viscosity, the deviatoric strain rate and the pressure. The pressure in the water is calculated as a function of the compression, and of the internal energy per unit volume, using the Mie-Grüneisen Equation of State. The required properties and constants of water were obtained from [63]. The same constitutive equation as in water and a Linear Polynomial Equation of State [64] were used to model the air. The mentioned Equation of State is linear in the internal energy and polynomial in the compression. Further details and the parameters used are given in [57].

The fluid-structure interaction, for both projectile/fluid and walls/fluid, is achieved by means of a penalty-based ALE-Lagrangian coupling algorithm implemented within LS-DYNA. This allows the fluid material to flow around the structure, but prevents its penetration into the mesh of the structure applying penalty forces to the fluid and the structure. The penalty forces are proportional to the penetration depth and penalty stiffness, behaving like a spring system.

The numerical model was validated with the experimental results of Varas et al. [56]. A complete and detailed description of the validation can be found in [57].

III. Analysis of the numerical results for fully filled tubes

The results obtained by means of the validated numerical model will be analyzed in order to achieve a greater understanding of the HRAM phenomenon. Due to the complexity of the phenomenon, the analysis of each result in an independent way is little enlightening, because most

of them are interrelated, so that each result can be used as an explanation of others. Therefore, initially a general case has been analyzed, showing all its results in order to explain certain aspects of the HRAM, which will be common to other cases. Subsequently some peculiarities observed in the remaining cases will be discussed.

On this section, the results concerning the case of a completely filled tube impacted at 900 m/s are analyzed. This analysis will help to have a complete and detailed view of the HRAM phenomenon. Similar energy balances and momenta could be found at other impact velocities.

It has to be mentioned that all curves in the following Figures of sections III and IV correspond to half a tube (obtained taking into account the symmetry of the quarter a tube model for the fully filled case) and half a projectile, so that the results can be easily compared.

A. Energy time histories

Figs. 4 and 5 depict the kinetic and internal energies of the different parts considered on the problem: projectile, water and the walls of the tube. The internal energy in the fluid must be associated to its volumetric strain due to the pressure increase, while it must be related to the plastic strain in the walls of the tube. Since the projectile has been modeled as elastic, its internal energy has not been taken into account on this analysis. The lateral wall referred in some of the following figures correspond to one of the walls of the tube where the projectile does not impact (Fig. 2, Left).

Figs. 4 and 5 show the existence of a first stage that corresponds to the passage of the projectile through the tube. In that stage, the kinetic energy of the projectile is transferred to the fluid and, through it, to the tank walls. The exit of the projectile occurs at t=0.3 ms. At that moment, the work done over the group tube-fluid ends and, from then, there is a transfer between the different terms of energy of structure and fluid.

Most of the energy is related to the fluid once the projectile exits the tank, as shown in Figs. 4 and 5. This is mainly due to the velocity that the projectile has transmitted to the water, rather than to the water pressure increase. After the exit of the projectile, however, the kinetic energy in the fluid decreases whereas the internal energy due to pressure keeps a constant and higher value for

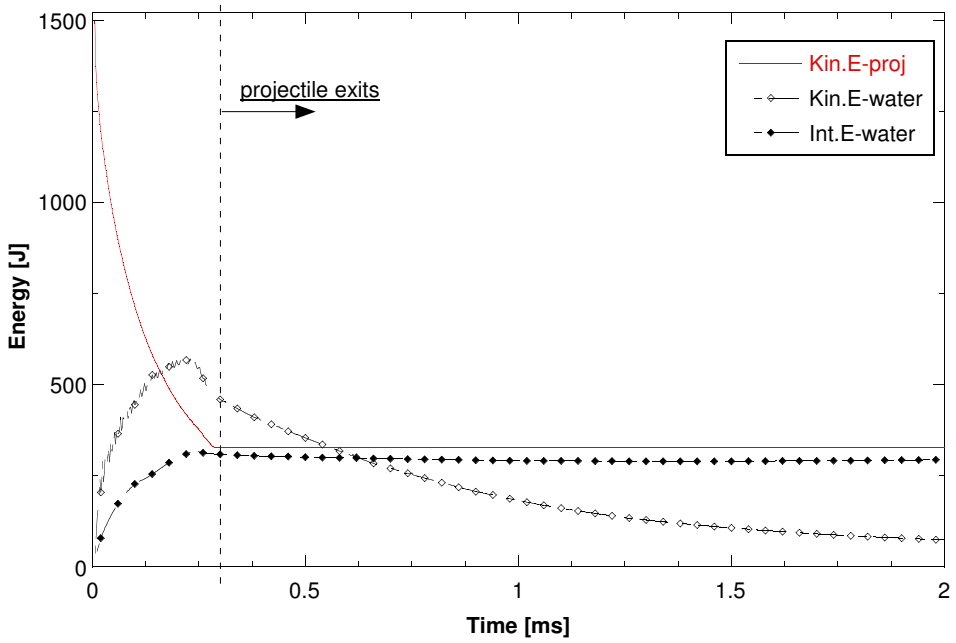

Fig. 4 Time history of energies in projectile and fluid. Fully filled tank and V=900 m/s.

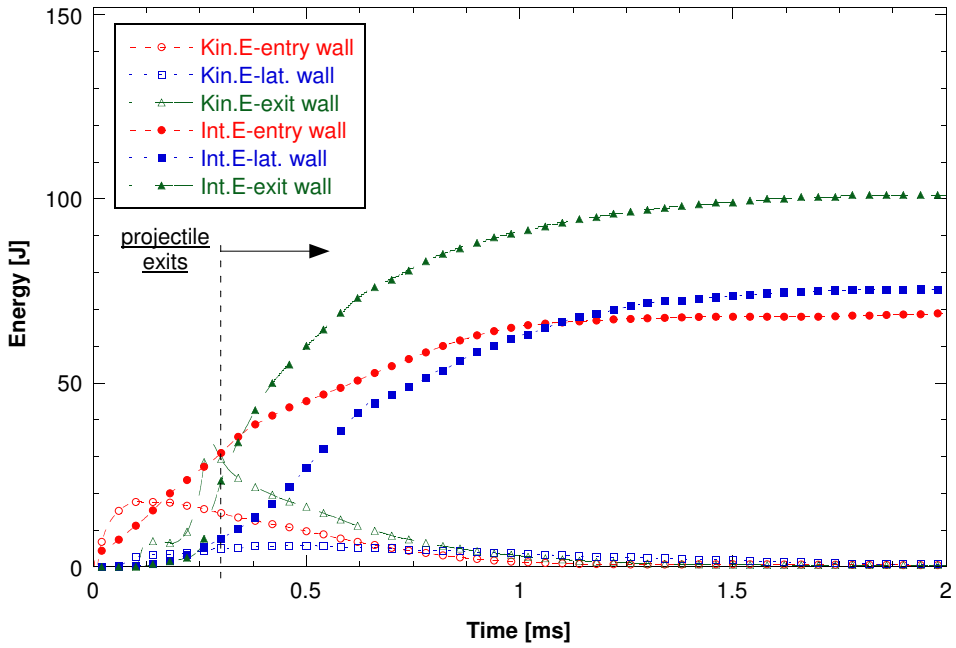

Fig. 5 Time history of energies in aluminium walls. Fully filled tank and V=900 m/s.

a much longer time than the one required by the projectile to pass through the tank. An increment of the internal energy of the water due to the cavity growth during the analyzed period could be expected; however this pressure increment is (due to the cavity growth) rapidly redistributed along

the tube. This assessment has been checked by means of the pressure contours in the fluid. The analysis of experimental images in [57] shows that the cavity grows very quickly during the projectile penetration on the fluid, while it slows down when the projectile is about to exit the tank. On the other hand, once the cavity reaches its largest size, it is maintained during a relative long time until the collapse process begins. It must be noted that, after the shock phase, the increase of energies in water is related to the formation of the cavity; its growth rate to the kinetic component and its size to the internal component or pressure. Thus, the numeric results of time history of energies in the fluid are consistent with the experimental observations of cavity evolution.

In Fig. 4 it can also be observed that the kinetic energy in the water begins to decrease before the exit of the projectile, which means that the fluid has already started to transmit part of its energy to the surrounding walls. On this first stage, the exit wall is the most affected, which would justify its pre-stressing before being impacted by the projectile. Later on it will be shown that the effect of the projectile contact on the entry wall is negligible for its acceleration and deformation.

For a better understanding of the structural response of the tube it is necessary to analyze in detail the internal and kinetic components of energy in the different walls. In Fig. 6 it can be observed that during the stage of projectile penetration, the kinetic energy of the walls is greater than the deformation energy, as happened in the fluid. This fact confirms the essentially dynamic nature of the first stage of HRAM, with the prevalence of inertial forces, against a behavior characterized by a more uniform pressure value in the fluid and slower walls deformation once the projectile has exited the tank.

B. Pressure contours

At the beginning of the cavity growth stage, the fluid pressure affects the entry wall, increasing its kinetic energy and deformation before any other wall of the tube. The lateral and the exit walls begin to accelerate when the pressure wave reaches each of them ($t\simeq$0.054 ms y $t\simeq$0.104 ms respectively). Thereafter, the kinetic energy increases up to $t\simeq$0.12 ms, instant in which the growth ceases both in the lateral and the exit wall. Later on the kinetic energy increases in the exit wall until a maximum shortly before the exit of the projectile. For a better understanding of this

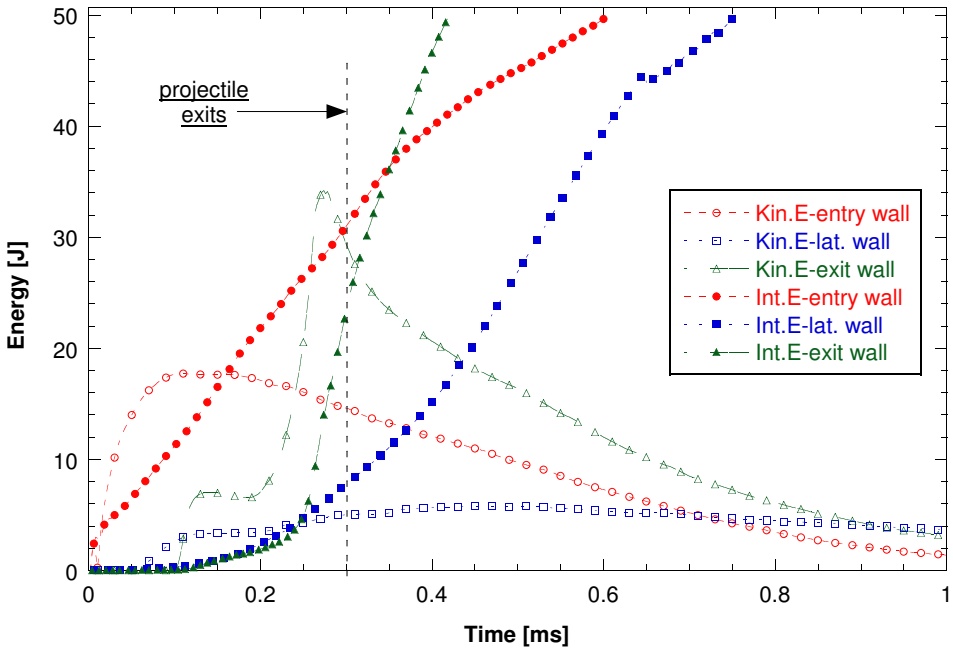

Fig. 6 Detail of the time history of energies in aluminium walls. Fully filled tank and V=900 m/s.

phenomenon, Fig. 7 shows the contours of pressure generated in the fluid during the advance of the projectile. It has to be noted that different contour scale has been used for each image; this allows a better visualization of overpressure zones.

The pressure contours clearly show the existence of two zones of overpressure [26]. The first one (zone "A" in Fig. 8) advances at the speed of sound in the fluid and is bounded between a spherical front centered on the impact point and a rarefaction front that appears as a result of the interaction with boundary conditions on the entry wall. The second zone (zone "B" in Fig. 8) advances in front of the projectile, at the same speed, and its value and extension decreases as the projectile decelerates [27]. Zone "A", due to its larger extension, affects both the exit and the lateral wall. Zone "B", with a smaller size area, mainly affects the exit wall when the projectile approaches it, and in a smaller extent the lateral walls. Fig. 7 clearly allows to observe the instants in which the overpressure wave "A" reaches both the lateral and the exit wall. Those instants match with the time determined from the kinetic energy curves for the same events. On $t \simeq 0.12\ ms$ the exit wall is no longer affected by the first over-pressure front, which would explain the plateau observed in the kinetic energy of the exit wall. Then, around $t=0.2\ ms$ the over-pressure front "B" begins to act

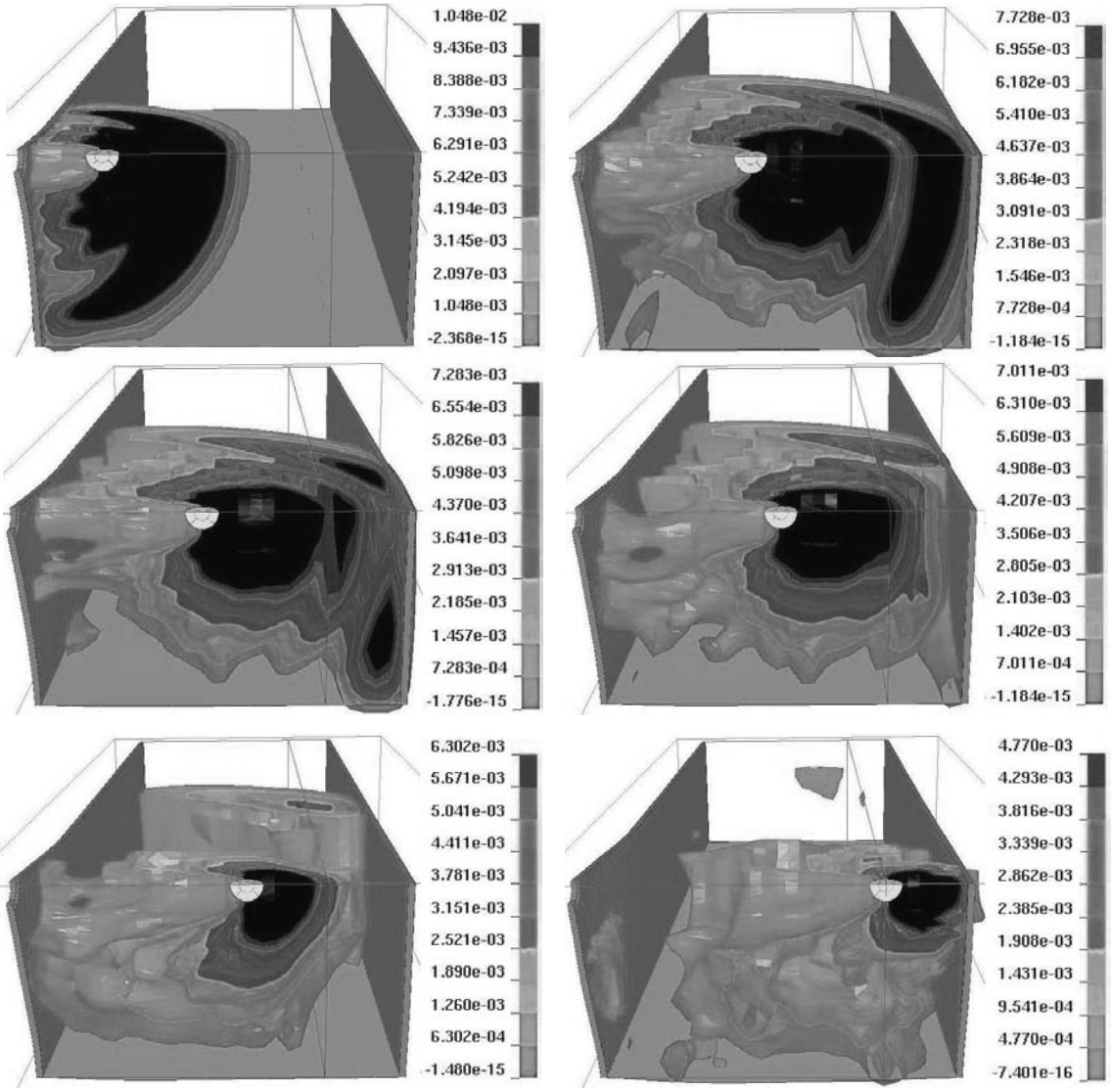

Fig. 7 Pressure contours in the fluid at 0.05, 0.10, 0.11, 0.12, 0.14 y 0.20 ms. Fully filled tank and V=900 m/s. Pressure units in GPa.

on the exit wall and causes a much higher kinetic energy rising than before. Therefore, the second over-pressure front seems to have more influence than the initial wave on the exit wall deformation. Finally, the maximum kinetic energy value on the exit wall occurs at the instant in which the projectile contacts it, decreasing from that moment and progressively turning into internal energy. It is worth to mention that the gap between the over-pressure zones "A" and "B" becomes more noticeable at lower impact velocities because the first front always moves at the same speed, while the second one travels at the projectile velocity. In those cases, the reduced growth phase of kinetic

energy on the entry and exit walls is longer. Regarding the lateral walls, they are affected by both over-pressure fronts “A” and “B” because of their proximity to the area of influence of the second front. On fuel tanks with lateral walls which are further away from the projectile trajectory, the second over-pressure front “B” should have no influence on their deformation.

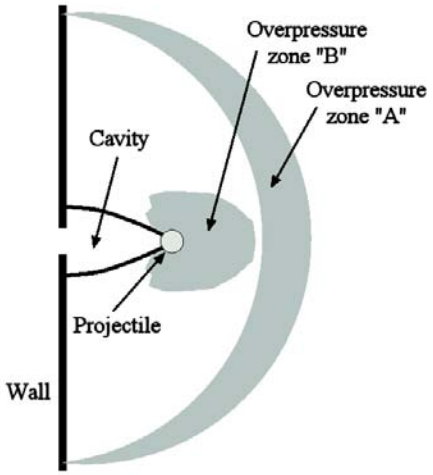

Fig. 8 Sketch of the overpressure zones in the fluid.

After the exit of the projectile, the walls continue their deformation due to the overpressure caused by the cavity formation. This overpressure is less intense than the overpressure generated by the two aforementioned fronts (as can be seen on the pressure values obtained both numerically and experimentally in the previous works of Varas et al. [56, 57]), but of greater temporal extent due to the fact that is not related neither to the sound waves propagation nor to the projectile advance. Therefore, its effect on the tube walls deformation is important (Fig. 5).

C. Momentum time histories

In addition to the pressure contours, the analysis of the momentum time history, both in the fluid and in the structure, allows to obtain information of interest for a better understanding of the HRAM phenomenon. From now on, the wall momenta that will be shown correspond to the perpendicular direction to each of them. Fig. 9 shows the momentum of projectile, water, entry wall and exit wall along the advance direction of the first one (Z-direction). First of all, it should be highlighted the negative sign for momentum on the entry wall, which can only be due to the pressure exerted by the fluid, bearing out the small effect of the contact of the projectile in what its

acceleration and deformations concerns. The entry wall begins to move from the beginning of the impact because of the over-pressure that the projectile penetration causes in the fluid. Regarding the exit wall, the momentum on Z-direction begins to rise when the mentioned wall is reached by the overpressure front "A" ($t \simeq 0.104\ ms$). Once the whole wave has reached the wall, the momentum increases in a moderate way until the overpressure "B" affects the wall ($t \simeq 0.2\ ms$), causing a high increase. When the projectile contacts the exit wall, the "B" front stops its effect on the wall and the momentum stops increasing. It is interesting to note that the stages of increasing momentum in the exit wall match with the stages of decreasing momentum in the fluid, proving the transfer of momentum between the water and the aluminum wall. After the exit of the projectile, the momentum in water increases again due to the exit of the fluid through the hole produced by the projectile.

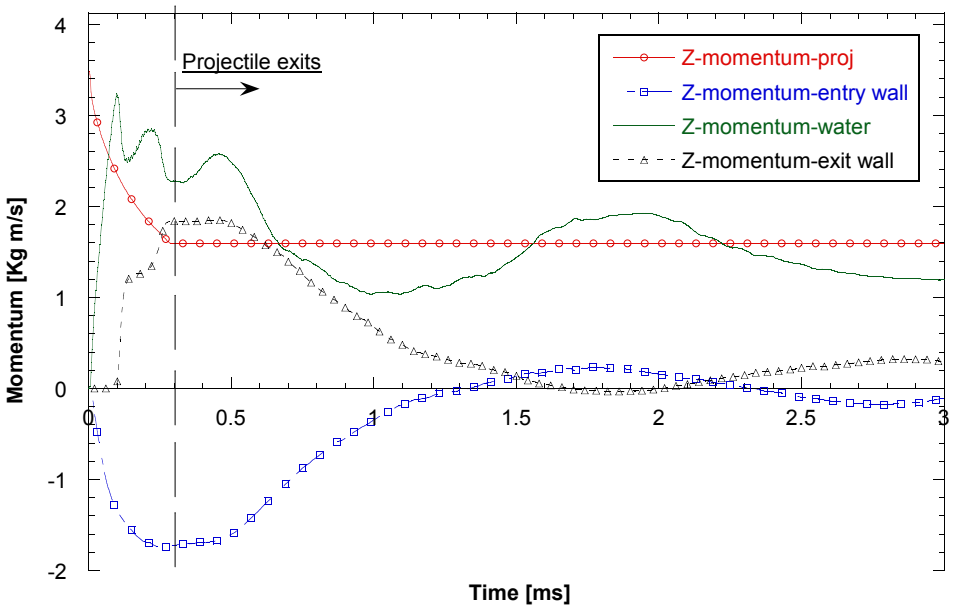

Fig. 9 Momentum of projectile, water, entry and exit walls in the direction of projectile advance. Fully filled tube and V=900 m/s.

Once the behavior of structure and fluid in the impact direction has been analyzed, the momentum of fluid and lateral walls in the perpendicular direction to the latter will be studied (Fig. 10). It has to be noted that the Y-momentum of water corresponds to the upper half of the volume (quarter of a tube) to avoid nil values due to symmetries. It can be observed that the values of

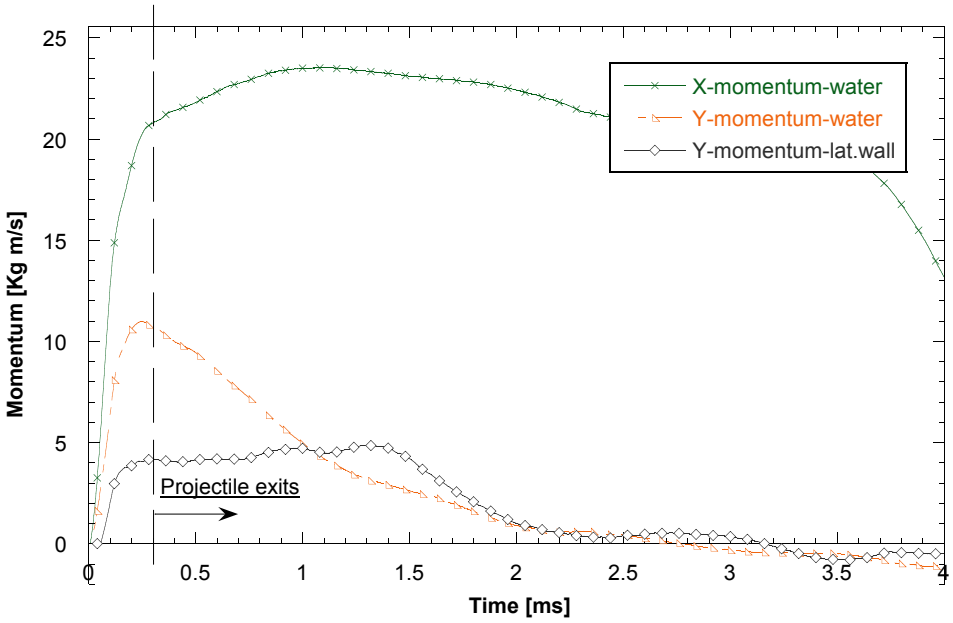

Fig. 10 Momentum of water and lateral wall in the perpendicular direction to projectile advance. Fully filled tube and V=900 m/s.

momentum in the fluid in the considered directions are higher than in the Z-direction due to the cavity formation, since a great amount of water is displaced essentially in a perpendicular direction to the path of the projectile. Particles located ahead of the projectile move at maximum velocity in Z-direction, but the volume that these particles take up is much smaller than the volume that the cavity moves in the other two directions (Fig. 11). Also, some differences in the evolution of the momentum in direction X and Y (perpendicular directions to projectile advance) in water are observed. The fluid continues its movement in X-direction due to the great distance of a boundary on that direction, while the momentum in the Y-direction decreases because of the presence of the lateral wall. The momentum on that wall begins to increase at $t \simeq 0.05\ ms$, instant in which the overpressure front "A" reaches the mentioned lateral wall (Fig. 7). When the influence of the "A" front finishes ($t \simeq 0.1\ ms$) a sudden change in the slope of the curve can be observed . In addition, it can also be seen that the momentum of the lateral wall in the Y-direction is larger than the momentum of entry and exit walls in the Z-direction (Fig. 9); this is due to the higher value of momentum of water in the Y-direction, with which the lateral wall exchanges momentum.

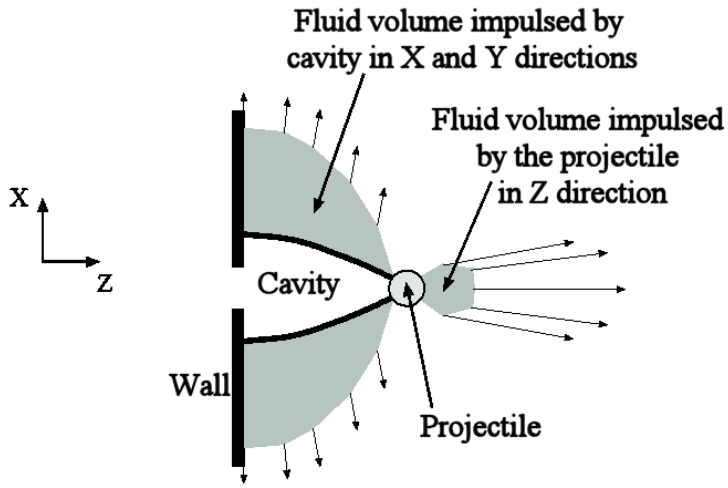

Fig. 11 Sketch of the velocity zones in the fluid.

The analysis performed in this section, regarding a completely filled tube impacted at 900 m/s, can be applied to the rest of the cases taking into account certain special features that are exposed in the next section for partially filled tubes.

IV. Analysis of the numerical results for partially filled tubes

In order to analyze the response of partially filled tubes impacted at different velocities, the results obtained for the case of a 75% filled tube impacted at 900 m/s will be shown. The qualitative aspects of this analysis can be extrapolated to the rest of configurations with partial filling.

A. Energy time histories

Figs. 12 and 13 show some special features compared to completely filled tubes. Unlike in 100% filled tubes, where the lateral walls are in contact with the fluid from the beginning and they behave in the same way to the impact, partially filled tubes show differences between the dry upper lateral wall (which is not in contact with water at the beginning) and the wet lower lateral wall (which is in contact with the fluid from the beginning).

The main difference of a partially filled case when compared to a completely filled tube is a slow decrease in the kinetic energy of water between $t\simeq 0.24$ ms and $t\simeq 0.624$ ms (Fig. 12). That is the time period from the instant in which the projectile contacts the exit wall to the instant in which the water reaches the dry upper lateral wall [56]. During this time the water loses kinetic

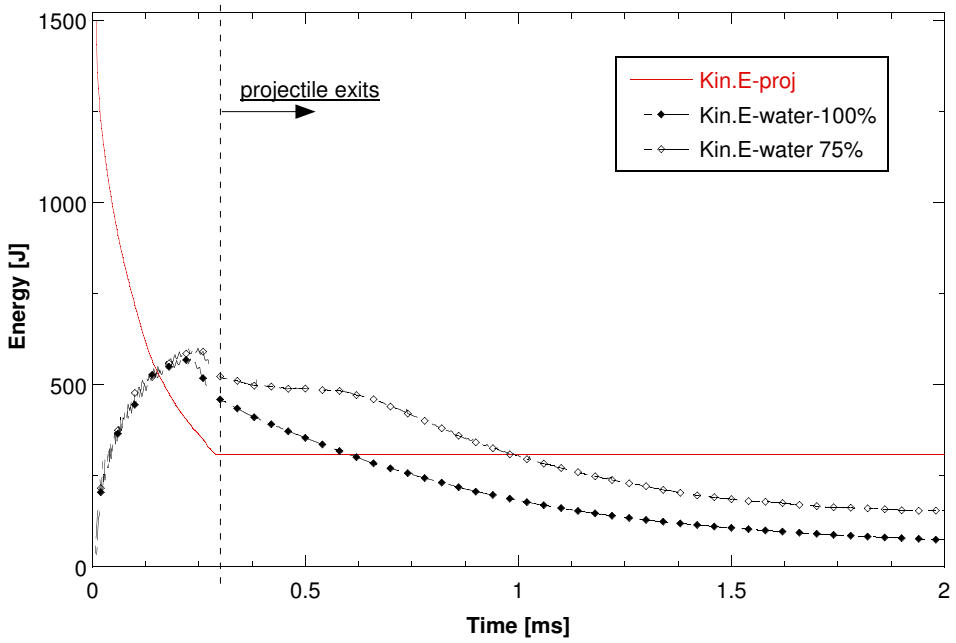

Fig. 12 Time history of kinetic energy in projectile and fluid. Completely and 75% filled tank, V=900 m/s.

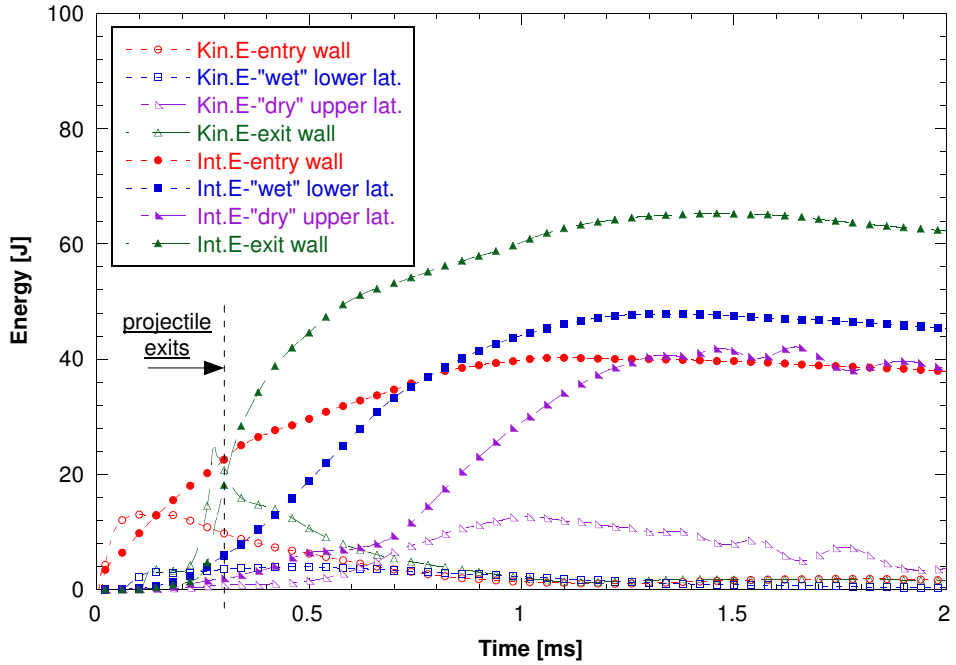

Fig. 13 Time history of energies in aluminium walls. 75% filled tank and V=900 m/s.

energy at a slower rate than if it was confined, due to the fact that the water layer generated over the projectile can freely move upwards to fill the existing void in the tube. Regarding the three

remaining walls: wet lower lateral wall, entry wall and exit wall (Fig. 13), it can be observed the same trends as in the case of completely filled tubes (Fig. 5), but with smaller values. This is due, firstly, to the lower pressure in the fluid, compared to a completely filled tank situation, as a result of the presence of an initial void volume. In addition, the entry and exit walls have less surface of contact with water, so the energy transmitted by the fluid is even lower. Thus, in a partially filled tank configuration, the HRAM affects in a smaller way the structure of the fuel tank.

Fig. 14 depicts in more detail the energy evolution in the walls. The kinetic energy in the dry upper lateral wall increases before water impacts it ($t \simeq 0.624\ ms$). This is because the mentioned wall begins to move towards the inside of the tube because of the outward deformation of the adjacent walls [55]. Once the water layer generated over the projectile reaches the dry upper wall and begins to transmit part of its energy, the kinetic component on the dry upper wall increases until it reaches a maximum value, which corresponds to the instant when the entire surface has been reached by the water. The other walls show similar trends as observed in the completely filled tube.

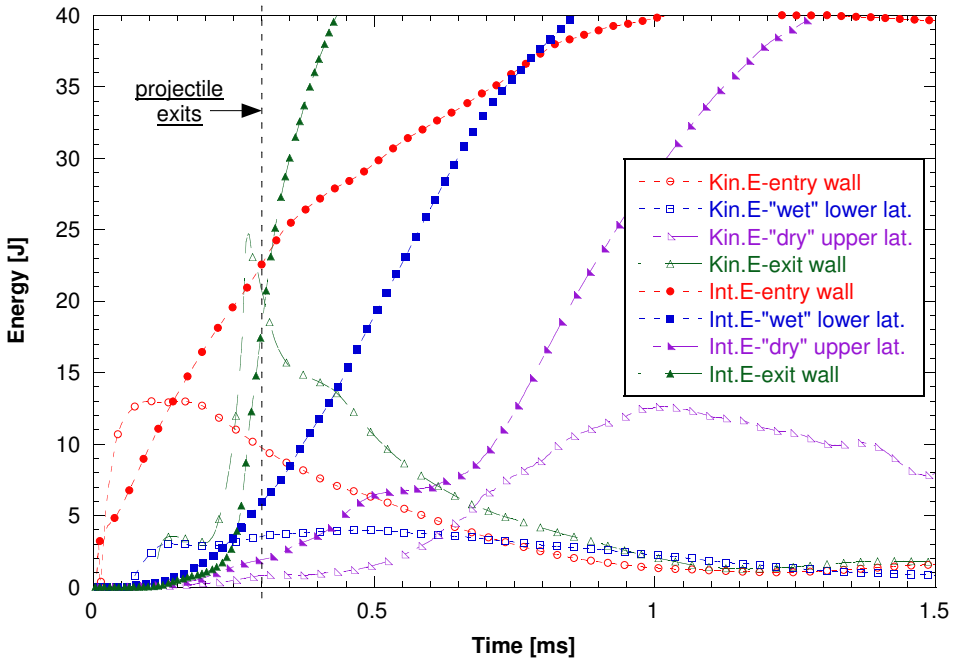

Fig. 14 Detail of the time history of energies in aluminium walls. 75% filled tank and V=900 m/s.

B. Momentum time histories

As in the case of completely filled tubes, Fig. 15 shows the momentum of projectile, water, entry and exit walls in the projectile advance direction in order to analyze the structural response of the tubes. The momenta for the partially filled cases correspond to the model of half tube used in the simulations. Similar trends to those corresponding for a completely filled tube (Fig. 9) are observed, so the analysis performed in that section can be perfectly applied in this case.

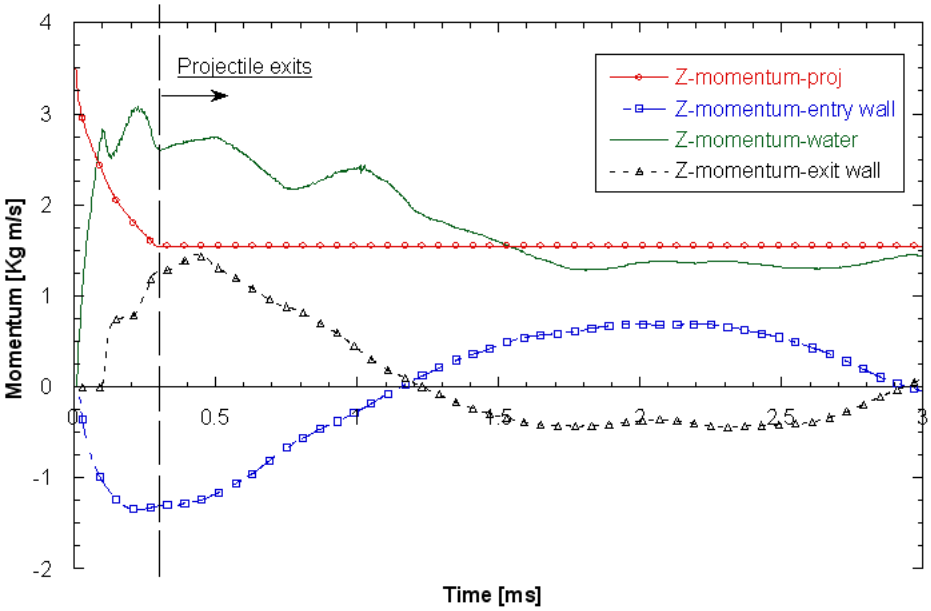

Fig. 15 Momentum of projectile, water, entry and exit walls in the direction of projectile advance. 75% filled tube and V=900 m/s.

Fig. 16 depicts the momentum of lateral walls and water in the perpendicular directions to projectile advance (X and Y). The momentum of fluid increases until the water contacts the dry upper lateral wall ($t \simeq 0.6\ ms$). Until that instant, the momentum of the dry wall has negative values due to the outward deformation of the adjacent walls that causes the motion of the dry wall towards the inside of the tube, as it was already mentioned. The upper dry wall changes its displacement direction when impacted by the fluid and so, the momentum towards the outside of the tube is increased. The momentum of the water in that direction (Y) stops increasing at around t=1 ms since the fluid is completely in contact with the dry upper wall. That time corresponds to the instant in which the kinetic energy of the upper dry wall is maximum. The momentum of the fluid

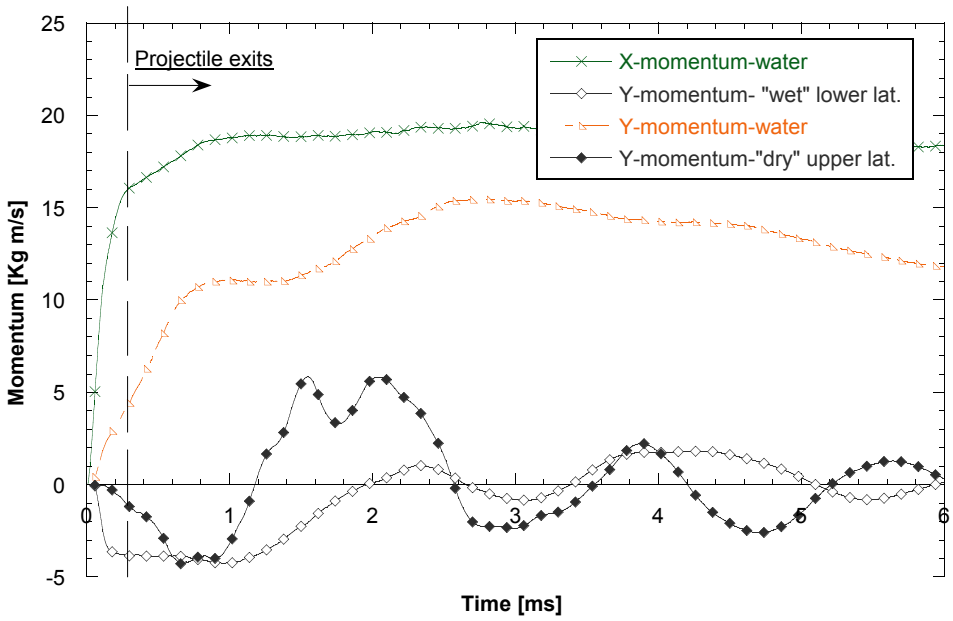

Fig. 16 Momentum of water and lateral walls in the perpendicular direction to projectile advance. 75% filled tank and V=900 m/s.

in that direction continues increasing because of the displacement of the water towards areas further from the impact trajectory.

Although a similar behavior has been observed in all cases of partially filled tubes, there is a difference in the kinetic energy of the dry upper wall. In the tube filled at 60% the maximum value of kinetic energy is reached before than in the case of the tube filled at 75%. This is due to the fact that, for a given impact velocity, it takes less time to the fluid to reach the dry upper wall when the tube has less fluid as it was observed experimental [56] and numerically [57] (Fig. 17).

V. Conclusions

The analysis of the results obtained from the numerical simulations has allowed to achieve a better understanding of the Hydrodynamic Ram. The tank walls deformation (effect) has been associated to the impact of the projectile (cause) by means of a detailed study of the interactions between these two solids and the fluid. This study has allowed to identify the process stages, the events which marked the beginning and the end of each of them and their respective influence in the permanent displacement of the structure. The main conclusions of this work could be summarized

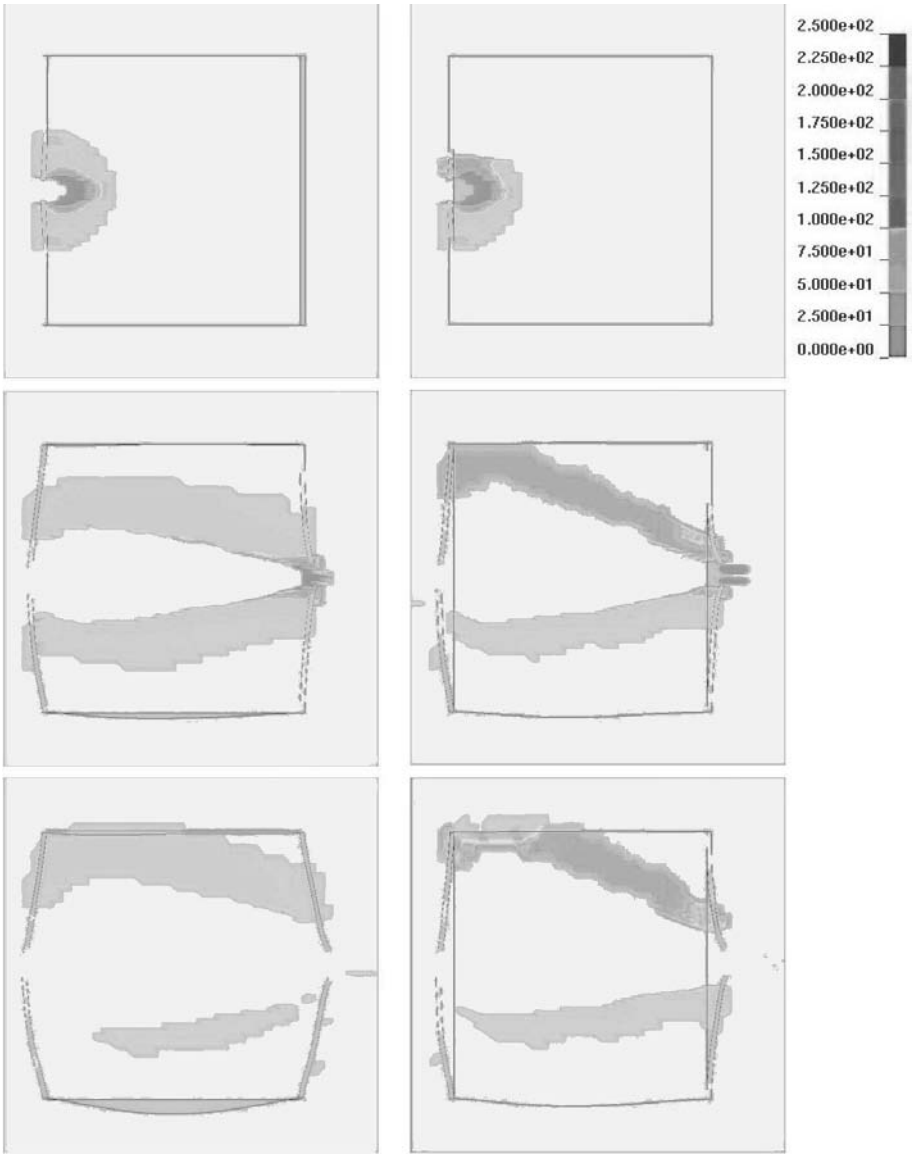

Fig. 17 Velocity contours, impact velocity 900 m/s. Left: 75%. Images at 0.03, 0.28 y 0.60 ms. Right: 60%. Images at 0.03, 0.30 y 0.38 ms.

as follows:

- The tube walls deformations are due to the fluid pressure; the effect of projectile contact on the aluminium walls is negligible. Only in the exit wall the impactor is responsible of the petalling.
- The first stage of the Hydrodynamic Ram phenomenon presents essentially a dynamic nature, with the prevalence of inertial forces, against a behavior characterized by a more uniform

pressure value in the fluid and slower walls deformation once the projectile has exited the tank.

- The exit wall is affected by the two overpressure fronts (A and B zones), while the lateral walls are affected mainly by the first front (A Zone); this results on smaller deformations on the lateral walls compared to the exit wall.

- The transferred momentum from the fluid to the walls during the drag and cavitation stages, is the most important factor in the tube deformation. In partial filled tubes, the fluid moves normally to the walls in regions close to the impact point, while it moves parallel to the walls in regions far from the impact point.

- The cavity growth generates a third overpressure stage inside the tube. Although its intensity is smaller than the other two overpressure fronts (A and B zones), its duration is longer in time causing the main plastic deformations of the walls.

- In partially fluid filled tubes, the plastic deformation of the dry lateral upper wall is due to the impact of the water layer created by the cavity growth. The magnitude of this deformation is proportional to the kinetic energy of this layer, which is higher for less filled tubes.

- The kinetic energy of the projectile is transferred to the structure by means of the cavity; hence any method which avoid the formation of the cavity, will diminish the structural damage and prevent the consequent catastrophic failure.

- The size of the two overpressure fronts, and so the effect on the surrounding zones, should be taken into account when designing the geometry and dimensions of a fuel tank which could be exposed to a high velocity impact.

Acknowledgements

This research was done with the financial support of the Spanish Ministry of Science and Innovation under Project references DPI/2008-06408 and DPI/2010-15123, and of the Region of Madrid and University Carlos III of Madrid under Project reference CCG10-UC3M/DPI-4694.

References

[1] Hinrichsen, R.L., Kurtz, A.G., Wang, J.T., Belcastro, C.M., Parks, J.L., "Modeling Projectile Damage in Transport Aircraft Wing Structures," AIAA Journal, Vol. 46, 2008, pp. 328-335.

[2] Santini, P., Palmieri, D., Marchetti, M., "Numerical simulation of fluid-structure interaction in aircraft fuel tanks subjected to hydrodynamic ram penetration," 21st ICAS Congress, Melbourne, Australia, 1998.

[3] Lundstrom, E.A., Stull, E., "Fluid dynamic analysis of hydraulic ram II (Results of experiments)," JTCG/AS 73-T-291, Joint Technical Coordinating Group/Aircraft Survivability.

[4] Lundstrom, E.A., "Fluid dynamic analysis of hydraulic ram," NWC TP 5227, Naval Weapons Center, 1971.

[5] Lundstrom, E.A., Fung, W.K., "Fluid dynamic analysis of hydraulic ram IV (Usert's manual for pressure wave generation model)," JTCG/AS 74-T-018,Joint Technical Coordinating Group/Aircraft Survivability, 1974.

[6] Ball, R.E., "Structural response of fluid-containing-tanks to penetrating projectiles (Hydraulic Ram). A comparison of experimental and analytical results," NPS-57B p76051, Naval Post Graduate School, Monterrey, California, 1976.

[7] Bates, K.S., Jr. "Aircraft fuel tank entry wall-projectile interaction studies," Master's thesis, NPS, 1973.

[8] Holm, D.P., "Hydraulic ram shock wave and cavitation effects on aircraft fuell cell survivability," Master's thesis, NPS, 1973.

[9] Soper, W.R., "Hydraulic ram studies," Master's thesis, NPS, 1973.

[10] Fuhs, A.E., Ball, R.E., Power HL. "Fy 73 hydraulic ram studies," NPS-57Fu74021, 1974.

[11] Mueller, L.S., "Experiments in hydraulic ram," Master's thesis, NPS, 1974.

[12] Kappel, L.C., "Hydraulic ram shock phase effects on fuel cell survivability," Master's thesis, NPS, 1974.

[13] Power, H.L., "Fy 74 experimental hydraulic ram studies," NPS-57Ph74081, 1974.

[14] Holm, C.M., "Hydraulic ram presure measurements," Master's thesis, NPS, 1974.

[15] Page, B., "Entry wall strain measurements during hydraulic ram," Master's thesis, NPS, 1975.

[16] Patterson, J.W., "Fuel cell pressure loading during hydraulic ram," Master's thesis, NPS, 1975.

[17] Power, H.L., "Fy 75 experimental hydraulic ram studies," NPS-57Ph75061, 1975.

[18] Bless, S.J., Fry, P.F., Barber, J.P., "Hydrodynamic Ram Driven Pressure Fields and Panel Displacements for High Velocity Spherical Fragments," in: Proceedings of the Hydrodynamic Ram Seminar, p. 37, May 1977.

[19] Avery, J.G.," AGARD, Design Manual for Impact Damage Tolerant Aircraft Structure," Technical Editing and Reproduction Ltd, London, UK, 1981.

[20] Lundstrom, E.A., Anderson, T., "Hydraulic ram model for high explosive ammunition, in: Symposium on Shock and Wave Propagation, Fluid-Structure Interaction and Structural Responses," ASME Pressure Vessels and Piping Conference, Honolulu, 1989.

[21] Sparks, C.E., Hinrichsen, R.L., Friedmann, D., "Comparisson ans validation of smooth particle hydrodynamic (SPH) and coupled euler lagrange (CEL) techniques for modelling hydrodynamic ram," in: 46th AIAA/ASME/ASCE/AHS/ASC Structures, Structural Dynamics & Materials Confer., Austin, Texas, 18-21 April 2005.

[22] Seddon, C.M., Moodie, K., Thyer, A.M., Moatamedi, M., "Preliminary analysis of fuel tank impact," International Journal of Crash, Vol. 9, 2004, pp. 237-244.

[23] Poehlmann-Martins, F., Gabrys, J., Souli, M., "Hydrodynamic ram analysis of non-exploding projectile impacting water," in: 2005 ASME Pressure Vessels and Piping Division Conference, Denver, Colorado, 17-21 July 2005.

[24] Nishida, M., Tanaka, K., "Experimental study of perforation and cracking of water-filled aluminum tubes impacted by steel spheres," International Journal of Impact Engineering, Vol. 32, 2006, pp. 2000-2016.

[25] Lecysyn, N., Dandrieux, A., Heymes, F., Slangen, P., Munier, L., Lapebie, E., Le Gallic, C., Dusserre, G., "Preliminary study of ballistic impact on an industrial tank: Projectile velocity decay," Journal of Loss Prevention in the Process Industries, Vol. 21, 2008, pp. 627-634.

[26] Lecysyn, N., Dandrieux, A., Heymes, F., Aprin, L., Slangen, P., Munier, L., Le Gallic, C., Dusserre, G., "Ballistic impact on an industrial tank: Study and modeling of consequences," Journal of Hazardous Materials, Vol. 172, 2009, pp. 587-594

[27] Lecysyn, N., Bony-Dandrieux, A., Aprin, L., Heymes, F., Slangen, P., Dusserre, G., Munier, L., Le Gallic, C., "Experimental study of hydraulic ram effects on a liquid storage tank: Analysis of overpressure and cavitation induced by a high-speed projectile," Journal of Hazardous Materials, Vol. 178, 2010, pp. 635-643.

[28] Disimile, P.J., Toy, N., Swanson, L., "A large-scale shadowgraph technique applied to hydrodynamic ram," Journal of Flow Visualization & Image Processing, Vol. 16, 2009, pp. 303-332.

[29] Disimile, P.J., Swanson, L.A., Toy, N., "The hydrodynamic ram pressure generated by spherical projectiles," International Journal of Impact Engineering, Vol. 36, 2009, pp. 821-829.

[30] Disimile, P.J., Davis, J., Toy, N., "Mitigation of shock waves within a liquid filled tank," International

Journal of Impact Engineering, Vol. 38, 2011, pp. 61-72.

[31] Ball, R.E., "A Computer Program for the Geometrically Nonlinear Static and Dynamic Analysis of Arbitrarily Loaded Shells of Revolution. Theory and Users Manual," NASA CR-1987.

[32] Ball, R.E., "Aircraft Fuel Tank Vulnerability to Hydraulic Ram: Modification of the Northrup Finite Element Computer Code BR-1 to include Fluid-Structure Interaction," Theory and Users Manual for BR-1HR, NPS-57B p74071, July 1974.

[33] Lundstrom, E.A., "Fluid/Structure Interaction in Hydraulic Ram," in: Proceedings of the Hydrodynamic Ram Seminar, May 1977, pp. 223-30.

[34] Herlin, W.M., Avery, J.G., "Hydraulic Ram Structural Response Computer Program (HRSR)," Boeing Co., Prepared under Contract N60530-80-C-0242 for Naval Weapons Center, China Lake, California.

[35] Freitas, C.J., Anderson Jr, C.E., Walker, J.D., Littlefield DL, "Hydrodynamic Ram: A Benchmark Suite," Symposium on Structures Under Extreme Loading Conditions, Vol. 325., New York, ASME 1996, pp. 63-74.

[36] Anghileri, M., Castelletti, L.-M.L., Tirelli, M., "Fluid-structure interaction of water filled tanks during the impact with the ground," International Journal of Impact Engineering, Vol. 31, 2005, pp. 235-254.

[37] Jarzab, W.W., Chwalinski, R., Pfrang, W.E., Tokar, G., "Fluid-structure interaction effects in tank structures due to sloshing and hydrodynamic ram Coupled Lagrangian-Eulerian simulations," Proc. International Conference: Spacecraft Structures and Mechanical Testing, Noordwijk, The Netherlands, 1988

[38] Souli, M., Olovsson, L., Do, I., "ALE and Fluid-Structure Interaction Capabilities in LS-DYNA," 7th International LS-DYNA Users Conference, Dearborn, Michigan, May 19-21, 2002.

[39] Fasanella, E.L., Boinott, R.L., Kellas, S., "Test and Analysis Correlation of High Speed Impacts of Ice Cylinders," 9th International LS-DYNA Users Conference, Dearborn, Michigan, June 4-6, 2006.

[40] Börvik, T., Hanssen, A.G., Langseth, M., Olovsson, L., "Response of structures to planar blast loads-A finite element engineering approach," Computers and Structures, Vol. 87, 2009, pp. 507-520.

[41] Lu, Y., Wang, Z., "Characterization of structural effects from above-ground explosion using coupled numerical simulation," Computers and Structures, Vol. 84, 2006, pp. 1729-1742.

[42] Kim, J.H., Shin, H.C., "Application of the ALE technique for underwater explosion analysis of a submarine liquefied oxygen tank," Ocean Engineering, Vol. 35, 2008, pp. 812-822.

[43] Marklund, P.O., Nilsson, L., "Simulation of airbag deployment usin a coupled fluid-structure approach," 7th International LS-DYNA Users Conference, Dearborn, Michigan, May 19-21, 2002.

[44] Koishi, M., Okano, T., Olovsson, L., Saito, H., Makino, M., "Hydroplaning simulation using fluid-

structure interaction in LS-DYNA," 9th International LS-DYNA Users Conference, Dearborn, Michigan, June 4-6, 2006.

[45] Hanssen, A.G., Girard, Y., Olovsson, L., Berstad, T., Langseth, M., "A numerical modelfor bird strike of aluminium foam-based sandwich panels," International Journal of Impact Engineering 2006, Vol. 32, pp. 1127-1144.

[46] Jenq, S.T., Hsiao, F.B., Lin, I.C., Zimcik, D.G., Nejad Ensan, M., "Simulation of a rigid plate hit by a cylindrical hemi-spherical tip-ended soft impactor," Computational Materials Science, Vol. 39, 2007, pp. 518-526.

[47] Zhang, A., Suzuki, K., "A comparative study of numerical simulations for fluid-structure interaction of liquid-filled tank during ship collision," Ocean Engineering, Vol. 34, 2007, pp. 645-652.

[48] Sauer, M., "Simulation of high velocity impact in fluid-filled containers using finite elements with adaptive coupling to smoothed particle hydrodynamics," International Journal of Impact Engineering, Vol. 38, 2011, pp. 511-520.

[49] Bathe, K.J., Zhang, H., Ji, S., "Finite element analysis of fluid flows fully coupled with structural interactions," Computers and Structures, Vol. 72, 1999, pp. 1-16.

[50] Unger, R., Haupt, M.C., Horst, P., "Application of Lagrange multipliers for coupled problems in fluid and structural interactions," Computers and Structures 2007, Vol. 85, pp. 796-809.

[51] Vierendels, J., Lanoye, L., Degroote, J., Verdonck, P., "Implicit coupling of partitioned fluid-structure interaction problems with reduced order models," Computers and Structures, Vol. 85, 2007, pp. 970-976.

[52] Kayser-Herold, O., Matthies, H.G., "A unified least-squares formulation for fluid-structure interaction problems," Computers and Structures, Vol. 85, 2007, pp. 998-1011.

[53] Tai, C.H., Liew, K.M., Zhao, Y., "Numerical simulation of 3D fluid-structure interaction flow using an immersed object method with overlapping grids," Computers and Structures, Vol. 85, 2007, pp. 749-762.

[54] Lee, K., Noguchi, H., Koshizuka, S., "Fluid-shell structure interaction analysis by coupled particle and finite element method," Computers and Structures, Vol. 85, 2007, pp. 688-697.

[55] Varas, D., López-Puente, J., Zaera, R., "Experimental study of CFRP fluid-filled tubes subjected to high-velocity impact," Composites Structures, Vol. 93, 2011, pp. 2598-2609.

[56] Varas, D., López-Puente, J., Zaera, R., "Experimental analysis of fluid filled aluminium tubes subjected to high velocity impact," International Journal of Impact Engineering, Vol. 36, 2009, pp. 81-91.

[57] Varas, D., Zaera, R., López-Puente, J., "Numerical modeling of the hydrodynamic ram phenomenon," International Journal of Impact Engineering, Vol 36, 2009, pp. 363-374.

[58] Varas, D., López-Puente, J., Zaera, R., "Numerical modelling of partially filled aircraft fuel tanks submitted to Hydrodynamic Ram," Aerospace Science and Technology, In Press.

[59] Johnson GR, Cook WH, A constitutive model and data for metals subjected to large strains, high strain rates, and temperatures, Proceedings of 7th Int. Symp., The Hague, The Nederlands, 1983, p.1-7.

[60] Karagiozova D, Jones N, Dynamic buckling of elastic-plastic square tubes under axial impact II: Structural response, International Journal of Impact Engineering 30, 2004, p. 167-192.

[61] Yang C C, Material Properties of Square Tube, The 9th Fundamental Scientific Conference of Chinese Armed Forces Academy, Taiwan, R.O.C., Vol. 1, ppB1 11, 2002.

[62] Vesenjak M, Matthaei M, Mullerschon H, Ren Z. Fluid models in LS-DYNA and their interaction with a structure in dynamic simulations, Proceedings of PVP2005. ASME Pressure Vessels and Piping Division Conference, Denver, 2005.

[63] Boyd R, Royles R, El-Deeb K M M, Simulation and validation of UNDEX phenomena relating to axisymmetric structures, 6th International LS-DYNA Users Conference Simulation 2000, Dearborn, Michigan, April 9-11, 2000.

[64] LS-DYNA KEYWORD USERt'S MANUAL, Nonlinear Dynamic Analysis of Structures, Version 971, Livermore Sotware Technology Corporation, May 2007.